AIP | The Journal of Chemical Physics

Dynamic mesoscale model of dipolar fluids via fluctuating hydrodynamics

Rasmus A. X. Persson, Nikolaos K. Voulgarakis, and Jhih-Wei Chu

Citation: The Journal of Chemical Physics **141**, 174105 (2014); doi: 10.1063/1.4900498
View online: http://dx.doi.org/10.1063/1.4900498
View Table of Contents: http://scitation.aip.org/content/aip/journal/jcp/141/17?ver=pdfcov
Published by the AIP Publishing

Dynamic mesoscale model of dipolar fluids via fluctuating hydrodynamics

Rasmus A. X. Persson,[1,2,a)] Nikolaos K. Voulgarakis,[3] and Jhih-Wei Chu[1,2,b)]
[1]*Institute of Bioinformatics and Systems Biology, National Chiao Tung University, Hsinchu 30068, Taiwan*
[2]*Department of Biological Science and Technology, National Chiao Tung University, Hsinchu 30068, Taiwan*
[3]*Department of Mathematics, Washington State University, Richland, Washington 99372, USA*

(Received 16 July 2014; accepted 15 October 2014; published online 4 November 2014)

Fluctuating hydrodynamics (FHD) is a general framework of mesoscopic modeling and simulation based on conservational laws and constitutive equations of linear and nonlinear responses. However, explicit representation of electrical forces in FHD has yet to appear. In this work, we devised an *Ansatz* for the dynamics of dipole moment densities that is linked with the Poisson equation of the electrical potential ϕ in coupling to the other equations of FHD. The resulting ϕ-FHD equations then serve as a platform for integrating the essential forces, including electrostatics in addition to hydrodynamics, pressure-volume equation of state, surface tension, and solvent-particle interactions that govern the emergent behaviors of molecular systems at an intermediate scale. This unique merit of ϕ-FHD is illustrated by showing that the water dielectric function and ion hydration free energies in homogeneous and heterogenous systems can be captured accurately via the mesoscopic simulation. Furthermore, we show that the field variables of ϕ-FHD can be mapped from the trajectory of an all-atom molecular dynamics simulation such that model development and parametrization can be based on the information obtained at a finer-grained scale. With the aforementioned multiscale capabilities and a spatial resolution as high as 5 Å, the ϕ-FHD equations represent a useful semi-explicit solvent model for the modeling and simulation of complex systems, such as biomolecular machines and nanofluidics. © *2014 AIP Publishing LLC*. [http://dx.doi.org/10.1063/1.4900498]

I. INTRODUCTION

For complex systems encountered in physics, chemistry, and biology, the behaviors of interest usually emerge from molecular interactions at an intermediate scale that spans from tens of nanometers to below the micrometer. Examples, to name a few, include the biological machineries of gene expression and biopolymer synthesis,[1,2] devices of energy transformation and storage,[3,4] as well as transporters of molecules and information across phase boundaries.[5,6] In general, the mesoscopic regime described above is too large for a fully atomistic description of functional activities to be practical but too small for systems to solely follow the averaged phenomena dictated by continuum mechanics. The aspects of molecular specificity and the constraints of physical laws thus need to be put together to comprehend such systems. Furthermore, an essential property for unusual features to emerge at the intermediate scale is thermal fluctuations that convolute the effects of different forces. To enable joint consideration of multifaceted factors, it is becoming increasingly clear that computer simulation is demanded as an indispensable complement to experimental methods.[7–9] In this regard, we recognize that a key objective of mesoscopic modeling and simulation is providing a theoretical platform to integrate the relevant mechanics for revealing how specific behaviors originate from molecular structures and interactions. Another requirement is that the representation needs to be sufficiently coarse grained (CG) for the model to be practically useful in capturing and explaining the main features of the system.

The commonly employed approaches of modeling a complex system at an intermediate scale can generally be divided into two categories. The first is coarse graining particles into particles.[10,11] Although the fundamental functional forms of intra- and inter-molecular potentials may still be retained at the level of united atoms, more drastic reduction of details often obscures the parameterization and interpretation of interaction potentials between CG particles.[10,11]

The second approach is coarse graining particles into fields for representing conservation laws and variational principles.[12,13] Irreversible responses ubiquitously encountered at the intermediate scale can be incorporated via the constitutive equations of the relevant types of fluxes, and the transport coefficients of which may also be measured experimentally. The effects of thermal noises can also be incorporated, for example, as in the fluctuating hydrodynamics (FHD) of Landau.[14,15] In adopting the Lagrangian viewpoint, conservational and constitutive laws may be translated into a particle-like dynamics to facilitate representation of complicated structures and non-uniform boundaries. Many methods of mesoscopic simulations are in this category,[16,17] including smoothed-particle hydrodynamics,[18,19] dissipative-particle dynamics,[20–22] and lattice-Boltzmann (LB) methods.[23,24] However, such forms of equations of motion often do not exactly satisfy the original conservational laws. Moreover, interpreting the dynamics of field variables as the equations of motion of particles inevitably requires specific assumptions that complicate generalization to more realistic scenarios such as multi-phase and multi-component flows.

a)Present address: Max-Planck-Institut für Kohlenforschung, Kaiser-Wilhelm-Platz 1, DE-45470 Mülheim an der Ruhr, Germany.
b)Electronic mail: jwchu@nctu.edu.tw

On the other hand, direct solution of FHD equations is a straightforward approach to impose conservation laws and linear response theories, especially with the recent advancement in numerical discretization schemes that even a grid size as small as 5 Å can be used to solve the FHD equations.[25–27] With the mapping operator that projects the positions and velocities of particles onto the field variables in different grid cells in space,[28,29] it can be shown that the equation of state and transport coefficients in the FHD equations can be calculated from the trajectories of all-atom MD simulations with special care of the finite sizes of molecules when a small grid size smaller than 10 Å is used for discretization.[26,27] This multiscale mapping from atomistic MD also applies to non-isothermal FHD equations.[30] The ability of resolving fluid flow at a small length scale also makes the FHD equations suitable for modeling interfacial flows.[31]

For more complicated problems that are required to resolve molecular structures, a hybrid FHD/MD scheme can be deduced to represent solvation and solvent-mediated interactions between particles.[32] In this case, the time propagation of field and particulate degrees of freedom are conducted together. Therefore, the hybrid FHD/MD scheme provides a platform to represent molecularly specific properties together with the universally required conservation laws. It was shown that using interaction potentials and forces between particles and fields, the hybrid FHD/MD scheme can simultaneously capture the behaviors of hydrodynamics and hydrophobicity.[32]

To serve as a general framework of mesoscopic simulation, though, an essential requirement is the ability to describe electrical forces. In the intermediate length scale, it is generally not known *a priori* the relative roles of different mechanics in contributing to the emergent behaviors of interest, since the specific structures of the system and thermal fluctuations tend to couple different forces in a highly non-trivial manner. It is thus important for mesoscopic simulation to jointly consider the impact of different physical interactions on the dynamics. In deterministic continuum mechanics, hydrodynamic equations for polarizable fluids can be derived rigorously[33] and a simplified form has been applied to describe the electrokinetic motions of charged colloidal particles[34–36] In the mesoscopic regime where stochastic effects become essential, incorporation of electrical forces in the FHD equations is yet to be developed for simulating electrokinetic phenomena at the nanoscale.

In this work, we devise a set of FHD equations to simulate the spatial and temporal variation of the electric potential (ϕ) due to fluctuating dipole moments and permanent charges in the fluid, and the resulting electrical forces are fed back to the momentum equations to affect the fluid flow. Unlike the approaches based on Onsager's reaction field[37,38] that treat the solvent as a dielectric continuum without transient dielectric responses, the ϕ-FHD equations developed here employ an *Ansatz* for the temporal evolution of electrical dipole fields. Therefore, in contrast to many of the fluid-dynamics based approaches[39] or the meanfield treatment,[40] the dielectric constant is not an input parameter to the ϕ-FHD model but an emergent property from the resulting statistics of dipole fluctuations.

Compared to the explicit[41,42] and implicit solvent[43–48] approaches, both widely used in all-atom based simulations,[49] ϕ-FHD can be regarded as a "semi-explicit" solvent with the mass, charge, and polarization densities of the solvent situating on grid cells of 5 Å as the default value. This length-scale of discretization can be changed depending on the specific needs of modeling but 5 Å is sufficiently large for the solvent flow to follow the continuum dynamics of the FHD equations and also adequately small to represent interfacial flows.[31]

For fluid flows at a charged or dipolar interface, responses to fluctuations in the electric field in the solvent would couple to changes in molecular structures at the surface in determining the overall dynamics. For molecular systems at the nanoscale, the fluctuations of charged or dipolar particles also depend on those of the solvent electric fields. In addition to electrostatics, other forces of hydrodynamics and thermodynamics jointly apply in giving rise to these phenomena. The introduction of ϕ-FHD equations presented in this work aims to develop a theoretical framework for integrating the physical forces relevant to mesoscopic simulation. In the presence of explicit charge densities and mass transfer equations, the ϕ-FHD equations can be readily applied to model electrokinetic processes.

In the following, the equations of ϕ-FHD we developed will first be discussed in detail. Magnetic effects[33] are not considered as in most molecular simulations. Next, the merit of combining electrical and other essential forces in a mesoscopic simulation model is illustrated by several non-trivial test cases. We also analyze the coarse graining of all-atom MD simulation to the field variables of ϕ-FHD for establishing that the model parametrization and development of which can incorporate information from a finer grained scale. Finally, the conclusion is presented.

II. FLUCTUATING HYDRODYNAMICS EQUATIONS FOR A DIELECTRIC SOLVENT (ϕ-FHD)

We let t denote time and $\mathbf{x}$ a location in space in the laboratory (Eulerian) frame associated with the solvent. For brevity, explicit labeling of the dependence of a symbol on its arguments is only done when extra clarity is needed. Apart from the occasional Cartesian index and "0" for vacuum permitivity, symbols pertaining to the solvent do not carry subscripts. We only employ subscripts on symbols related to dissolved components. Furthermore, we denote the absolute temperature by T and the Boltzmann constant by k_B.

The fluid system satisfies the continuity equation of mass density ρ:

$$\frac{\partial \rho}{\partial t} = -\nabla \cdot \mathbf{g}. \tag{1}$$

Here, $\mathbf{g}$ is the momentum density and it is related to the velocity field $\mathbf{v}$ through $\mathbf{g} = \rho\mathbf{v}$. The law of conservation of momentum dictates the dynamics of $\mathbf{g}$ as

$$\frac{\partial \mathbf{g}}{\partial t} = -\nabla \cdot (\mathbf{gv}) - \nabla \cdot (\mathbf{R} + \mathbf{D} + \mathbf{D}^s). \tag{2}$$

In Eq. (2), $\mathbf{R}$ is the reversible stress tensor, $\mathbf{D}$ is the dissipative stress tensor, and $\mathbf{D}^s$ is the fluctuating stress tensor mandated

by the fluctuation-dissipation (FD) theorem. Using a simple equation of state with the speed of sound as the parameter (more complicated equation of state can be used if necessary) and denoting the electrostatic potential by ϕ, it can be shown that $\mathbf{R}$ is

$$\nabla \cdot \mathbf{R} = c^2 \nabla \rho + \widetilde{n} \nabla \phi. \tag{3}$$

A formal derivation for the second term is outlined in the Appendix. In Eq. (3), $\widetilde{n}$ is the charge density. For the dissipative stress tensor, we assume that the fluid is Newtonian although more complicated constitutive equations can also be implemented if desired. As a result,

$$\mathbf{D} = \eta^{\mathrm{S}}(\nabla \mathbf{v} + (\nabla \mathbf{v})^{\mathrm{T}}) + \left(\eta^{\mathrm{B}} - \frac{2}{3}\eta^{\mathrm{S}}\right)(\nabla \cdot \mathbf{v})\mathbf{I}. \tag{4}$$

Here, η^{B} and η^{S} are coefficients of bulk and shear viscosity, respectively. The symbol $\mathbf{I}$ represents the identity tensor. The fluctuating stress tensor describes thermal fluctuations in momentum fields according to the mathematical form of $\mathbf{D}$ to achieve the fluctuation-dissipation balance. From Eq. (4), we have

$$\begin{aligned}\left\langle D^{\mathrm{s}}_{ij}(t, \mathbf{x}) D^{\mathrm{s}}_{kl}(t', \mathbf{x}')\right\rangle = 2k_{\mathrm{B}}T\delta(t - t')\delta(\mathbf{x} - \mathbf{x}') \\ \times\Big[\eta^{\mathrm{S}}(\delta_{ik}\delta_{jl} + \delta_{il}\delta_{jk}) \\ + \left(\eta^{\mathrm{B}} - \frac{2}{3}\eta^{\mathrm{S}}\right)\delta_{ij}\delta_{kl}\Big].\end{aligned} \tag{5}$$

In this equation, the covariances between each element of the second-rank tensor $\mathbf{D}^{\mathrm{s}}$ at times t, t' and locations $\mathbf{x}, \mathbf{x}'$ are specified.

In an ideal dielectric solvent, the presence of external electric fields do not induce net electric currents but polarizes the solvent to gain the polarization charge density as

$$\widetilde{n} = -\nabla \cdot \mathbf{p}. \tag{6}$$

In this equation, $\mathbf{p}$ denotes the density of the induced dipole moment, and the assumption that no higher-order electrostatic moments from the quadrupole and up contribute to the polarization density has been made. As such, the fluid responds only to the local electrostatic field $\nabla\phi$. Introducing the dipole polarizability α, the local electrostatic energy density can be defined up to an arbitrary constant as

$$u(\mathbf{p}) = \mathbf{p} \cdot \nabla\phi + \frac{\mathbf{p} \cdot \mathbf{p}}{2n\alpha}. \tag{7}$$

Here, n is the solvent number density. Minimizing this electrostatic energy density with respect to $\mathbf{p}$ yields the equilibrium polarization density as the following expression that is defined as the constitutive equation of polarization:

$$\mathbf{p}(\mathbf{x}) = -\alpha n(\mathbf{x}) \nabla\phi(\mathbf{x}). \tag{8}$$

For simplicity, we assume that α is constant with respect to $\nabla\phi(\mathbf{x})$, but this treatment is not a strict limitation and an expansion of α in hyperpolarizabilities may be implemented straightforwardly. The polarization charge densities resulting from Eq. (6) are then used to determine ϕ through the Poisson equation:

$$\nabla^2\phi = -\frac{\widetilde{n}}{\varepsilon_0}. \tag{9}$$

Here and in the following, we denote the vacuum permittivity by ε_0.

The local polarization density $\mathbf{p}$ is a continuum representation of the charge distributions in the fluid. However, since the continuum is discretized over minute fluid cells of 5 Å in solving the ϕ-FHD equations, $\mathbf{p}$ can only be resolved as the average in each grid cell. This average fluctuates under the thermal motion of the contributing molecules which in a fully atomistic MD simulation is determined by the equations of motion and the parameters of the potential energy function. In the mesoscopic model of ϕ-FHD, the resolution of resolving forces is limited by the grid cell size of choice. In this case, we employ random thermal noises to represent the effects of the missing details in each grid cell on its dipole moment. Equation (7) discussed earlier describes dipole-dipole interactions between grid cells. This strategy is analogous to the thermostatting of particle-based simulation methods,[50] such as in molecular dynamics and dissipative particle dynamics.[20–22]

Combining the considerations discussed above, we propose the following *Ansatz* that uses the form of an over-damped Langevin equation for the dynamics of the dipole moment densities in grid cells:

$$\left(\frac{\partial \mathbf{p}}{\partial t}\right) = -\eta\left\{\nabla\phi + \frac{\mathbf{p}}{n\alpha}\right\} + \mathbf{b}(\mathbf{x}, t). \tag{10}$$

Terms in the parenthesis of the RHS of Eq. (10) represent the deterministic forces for the responses of the dipole moment densities. The time scale for the forces to affect dynamics is determined by the mobility coefficient η, which in the analogy of particle dynamics is related to solvent viscosity.[51] Determination of this transport coefficient for the dipole moment densities will be discussed later. For the deterministic forces to govern the static properties of $\mathbf{p}$ as in the over-damped Langevin dynamics of particles, $\mathbf{b}(\mathbf{x}, t)$ takes the form as prescribed by the fluctuation-dissipation theorem:

$$\langle b_i(\mathbf{x}, t) b_{i'}(\mathbf{x}', t')\rangle = 2k_{\mathrm{B}}T\eta\delta_{ii'}\delta(\mathbf{x} - \mathbf{x}')\delta(t - t'). \tag{11}$$

Therefore, the average polarization density will follow the constitutive equation of Eq. (8) if $\nabla\phi$ is a steady external electric field given sufficient time for the noise due to thermal fluctuations to average out. The η parameter, on the other hand, determines the time scale of reaching the equilibrium.

Equation (10) is coupled to the rest of the FHD equations through the reversible stress tensor $\mathbf{R}$ and is thus consistent with the principles of the conservation laws of FHD. Furthermore, in the presence of fluid flow, an advection term may be added to Eq. (3):

$$\frac{\partial \mathbf{p}}{\partial t} = -\nabla \cdot (\mathbf{p}\mathbf{v}) - \eta\left\{\nabla\phi + \frac{\mathbf{p}}{n\alpha}\right\} + \mathbf{b}(\mathbf{x}, t). \tag{12}$$

Nevertheless, numerical calculations indicate that the advective term does not play a significant role in the regime of ϕ-FHD of small grid size and high solvent viscosity, i.e., low Reynolds number, as expected.

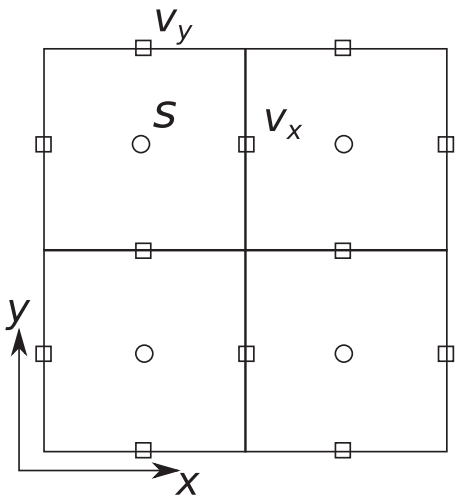

FIG. 1. Schematic illustration of the staggered discretization scheme. Scalars (denoted generically by S in the figure) are calculated and stored at cell centers, whereas vectors (components denoted by v_x and v_y in the figure) are calculated and stored at cell faces, one for each Cartesian component.

A. Numerical solution of the ϕ-FHD equations

The ϕ-FHD equations presented above can be solved by discretizing the simulation space into N_c cubic grid cells, and each cell has the volume of $V_c = d_c^3$. Periodic boundary conditions were applied in all three directions. The "staggered" scheme of finite differences[26] was employed, in which scalar fields such as mass densities, electrostatic potential, etc., are calculated and stored at cell centers, whereas vector fields such as the gradients of scalar fields are calculated by finite differences at cell faces. A schematic illustration is shown in Figure 1.

In this work, we consider water as the solvent and unless noted otherwise, the following parameters are used: $c = 13.937$ ps^{-1} Å, $\eta^B = 19.204$ amu ps^{-1} Å^{-1}, and $\eta^S = 53.858$ amu ps^{-1} Å^{-1}.[32] A second-order Euler predictor-corrector integrator was employed in all simulations with a time step of 5 fs. The electrostatic potential was obtained by a fast Fourier solver of Poisson's equation using the Singleton[52] algorithm. In all simulations that include thermal fluctuations, the temperature was set to 300 K. Averages were sampled over 2 ns trajectories.

Since the electrostatic coupling in Eq. (3) stems from the stochastic variable $\widetilde{n}$, the combination of a finite system and finite resolution gives rise to a non-zero stochastic contribution to the total electrical force acting on the entire system even if it is charge neutral. If unchecked, this minute residual force will lead to a very small but nonzero Brownian drift of the system during the simulation. To ensure the conservation of total linear momentum, we impose the explicit constraint

$$\frac{\partial}{\partial t}\int_V \mathbf{g}(\mathbf{x})d^3\mathbf{x} = 0 \tag{13}$$

by adding a constraint force $\lambda(t)$ to the equation of motion, so that it reads

$$\frac{\partial \mathbf{g}}{\partial t} = -\nabla\cdot(\mathbf{gv}) - \nabla\cdot\left(\mathbf{R}+\mathbf{D}+\mathbf{D}^s\right) + \lambda(t). \tag{14}$$

By combining this augmented equation of motion with the constraint of Eq. (13), we find the explicit form of the constraint force:

$$\lambda(t) = -\frac{1}{V}\int_V \{-\nabla\cdot(\mathbf{gv}) - \nabla\cdot(\mathbf{R}+\mathbf{D}+\mathbf{D}^s)\}d^3\mathbf{x}. \tag{15}$$

It is important to stress that Eqs. (13)–(15) are a numerical correction to the non-zero noise in a finite stochastic system that decays square-rootly with system size. Similar procedures are also common in molecular dynamics simulations.

The system state of a FHD simulation is specified by the mass, momentum, and polarization densities of all grid cells according to Figure 1. With the thermodynamic temperature set at value T, the numerical algorithm propagates the ϕ-FHD equations presented above in time. For clarity, the predictor-corrector scheme of moving forward a small time increment Δt is presented for the equations of the system in the following:

1. Calculate $\widetilde{n}$ from $\mathbf{p}$ by finite differences between nearest neighbors through Eq. (6). Since $\mathbf{p}$ is a vector stored at cell faces as the momentum density vectors, $\widetilde{n}$ is calculated at cell centers like the mass densities.
2. Calculate $\nabla\cdot\mathbf{g}$ via finite differences; calculate the non-electrostatic part of the reversible stress tensor $\mathbf{R}$ and the dissipative stress tensor $\mathbf{D}$ via the equation of state, Eq. (3) and the constitutive equation, Eq. (4), respectively.
3. Generate a random tensor $\mathbf{D}^s$ subject to the fluctuation-dissipation conditions stated above at the temperature T via Eq. (5).
4. Calculate ϕ by solving Eq. (9); ϕ is stored at cell centers, collocated with $\widetilde{n}$.
5. Generate a random vector $\mathbf{b}$ subject to the fluctuation-dissipation conditions stated above at the temperature T via Eq. (11).
6. Calculate $\partial\mathbf{p}/\partial t$ according to Eq. (10), $\partial\mathbf{g}/\partial t$ according to Eq. (2), and $\partial\rho/\partial t$ according to Eq. (1).
7. Calculate the predictors of state variables: $\mathbf{p}' = \mathbf{p} + \Delta t\partial\mathbf{p}/\partial t$; $\mathbf{g}' = \mathbf{g} + \Delta t\partial\mathbf{g}/\partial t$; $\rho' = \rho + \Delta t\partial\rho/\partial t$. The number density n' is proportional to the mass density ρ' through the solvent molecular weight.
8. Calculate $\partial\mathbf{p}'/\partial t$, $\partial g'/\partial t$, and $\partial\rho'/\partial t$ by repeating steps 1–10 with $\mathbf{p}'$, $\mathbf{g}'$, and ρ'.
9. Calculate state variables in the next time step via the corrector: $\mathbf{p} \leftarrow \mathbf{p} + 0.5(\partial\mathbf{p}'/\partial t + \partial\mathbf{p}/\partial t)\Delta t$; $\mathbf{g} \leftarrow \mathbf{g} + 0.5(\partial\mathbf{g}'/\partial t + \partial\mathbf{p}/\partial t)\Delta t$; $\rho \leftarrow \rho + 0.5(\partial\rho'/\partial t + \partial\rho/\partial t)\Delta t$. The number density n is then determined from the newly calculated ρ.

Therefore, all different physical quantities are updated together with time.

III. RESULTS AND DISCUSSION

In this section, the ϕ-FHD equations are applied to several model systems to illustrate the capability of integrating essential forces in mesoscopic scale simulation. First, the solvent dielectric function of ϕ-FHD is characterized and compared with the results of experimental measurements. Second,

we calculate the solvation free energy of ions to examine the accuracy that can be achieved by putting together the relevant interactions in simulation. We also simulate the distribution of ions of different sizes in a nanoscale droplet to illustrate that the ϕ-FHD framework has the potential as a general tool in modeling complex systems. Finally, coarse graining from all-atom MD simulations is analyzed to show that the information obtained in a finer grained scale can also be utilized to develop the ϕ-FHD model.

A. Solvent dielectric function

The complex dielectric function quantifies the dielectric response of the solvent to a time-varying external electric field. The zero-frequency value of this function represents the equilibrium response and is typically referred to as the static dielectric constant. If the polarization density p along an axis has been achieved due to an externally applied electric field E, the static dielectric constant is defined as

$$\widehat{\varepsilon}(0) = 1 + \frac{p}{\varepsilon_0 E}. \tag{16}$$

In general, the dielectric function $\widehat{\varepsilon}(\nu)$ is frequency (ν) dependent. Here, we show that the ϕ-FHD equations presented in the last section quantitatively describe the profiles of $\widehat{\varepsilon}(\nu)$ of water measured experimentally. Direct calculations of $\widehat{\varepsilon}(\nu)$ from all-atom MD simulations would suffer from high noise-to-signal ratio and are yet to appear to the best of our knowledge.

We consider a simulation box of $61.5 \times 61.5 \times 61.5$ Å^3 divided into $N_c = 12^3$ cubic grid cells. Each grid cell thus has a size of $d_c = 5.125$ Å. The results reported here are insensitive to the values of N_c used in the simulation within the sampled range of 8^3 to 16^3. The equilibrium density of water is $\rho = 0.998$ g/cm^3 in the ϕ-FHD simulations, and the temperature of the thermal fluctuations in the fluid flow was set to 300 K. To determine $\widehat{\varepsilon}(\nu)$, a constant electric field E along the z direction is applied and the resulting p value along this direction is tracked in time. In these calculations, the thermal fluctuations of the polarization density are turned off ($\mathbf{b} \equiv 0$ in Eq. (10)) so as to directly approach the value of the statistical average. In the presence of the external field, the equation of motion for the polarization density is modified to

$$\frac{\partial \mathbf{p}}{\partial t} = -\nabla \cdot (\mathbf{pv}) - \eta \left(\nabla \phi - \mathbf{E}_{\text{ext}} + \frac{\mathbf{p}}{n\alpha} \right) + \mathbf{b}. \tag{17}$$

The other FHD equations remain unchanged. Here, $\mathbf{E}_{\text{ext}}$ is the homogeneous (i.e., constant) external electric field. After equilibration in this constant field, it is turned off to observe the dielectric relaxation of the fluid. All other equations are the same as those described in Sec. II.

After a sufficiently long time, the polarization density in the fluid equilibrates and satisfies Eq. (16). By matching the experimental value[53] of the static dielectric constant, the value of α can be determined unambiguously. This procedure yielded $\alpha = 1.325 \times 10^{-3}$ amu^{-1} e^2 ps^2. Keeping α fixed at this value, the calculations were repeated at various solvent densities to explore if the density dependency of the static dielectric constant of water can be captured by the ϕ-FHD model. Comparison with experimental data[54] in Figure 2 indicates that the $\widehat{\varepsilon}(0)$ versus ρ trend is well captured without any additional fitting. Since the α value is fit only at the lowest density, this result indicates that Eq. (8) is a good approximation for modeling the static dielectric response of water.

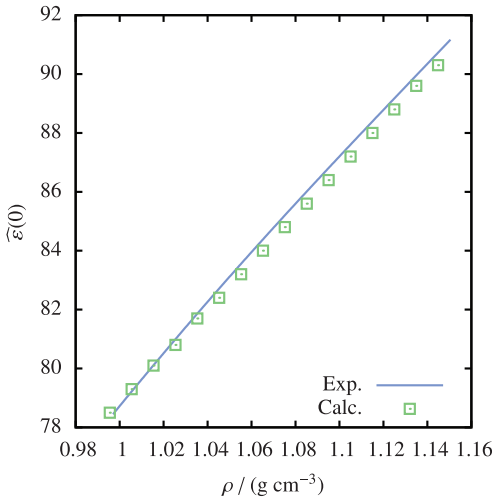

FIG. 2. Comparison of the calculated and experimental density dependence of $\widehat{\varepsilon}(0)$ for water for densities corresponding to pressures from 0.1 up to 500 MPa. The experimental curve is from the fit of Ref. 54.

The other ϕ-FHD parameter in Eq. (10) or the numerically equivalent in Eq. (12) that governs solvent polarization is η. To assess its effects, the external field E was instantly switched off after the steady value of $\mathbf{p}$ was reached and the time dependence of the polarization density $\mathbf{p}(t)$ decaying to zero was tracked at intervals of 2 ps. The Fourier transform of $\mathbf{p}(t)$ yielded the frequency-dependent complex susceptibility function $\widehat{\chi}(\nu) = \widehat{\varepsilon}(\nu) - 1$ up to a normalization constant that was found through the continuity of $\widehat{\varepsilon}(\nu)$ in the limit $\nu \to 0$. A fit of the calculated $\widehat{\varepsilon}(\nu)$ with the parameter $\eta = 4.90 \times 10^{-6}$ amu^{-1} e^2 ps Å^{-4} compared with an accurate multiparameter representation fitted to experiments[53] is shown in Figure 3. The comparison is focused in the

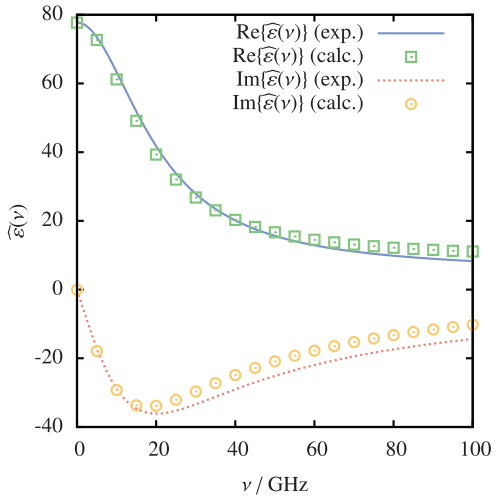

FIG. 3. Comparison of the experimental complex dielectric function of pure water and the calculated one. The experimental curves are taken from the multiparameter experimental fit of Ref. 53.

microwave region of the dielectric spectrum where the experimental data in Ref. 53 is the most reliable. For both the real and imaginary parts of $\widehat{\varepsilon}(\nu)$, the agreement of ϕ-FHD simulations with experimental profiles is clear. The deviation only becomes noticeable at higher frequencies, for which the overdamped Langevin *Ansatz* is slightly less tenable. Therefore, the dynamics *Ansatz* for dipole moment densities is consistent with the dielectric responses of water and can capture the frequency-dependent behaviors of the dielectric function up to the microwave region. Expanding the model by introducing an extra parameter of effective mass to describe inertial effects, i.e., higher-frequency responses, is thus not considered. This consistency forms the basis of determining the transport coefficient η from the observed phenomena, following the convention in the analysis of other types of transport phenomena. Based on this result, we also anticipate that the dynamic dielectric response of the solvent due to interactions with solutes may be captured by the ϕ-FHD model.

B. Simulation of ion hydration with the ϕ-FHD equations

The equations of ϕ-FHD presented in Sec. II describe fluid flow coupled with the dynamics of polarization densities, hence capturing both the hydrodynamic and electrostatic responses of the solvent. Since hydrophobic couplings can also be incorporated, an important test case is whether the interactions of solute particles such as ions with the solvent can be described under the ϕ-FHD framework. In particular, we calculate the solvation free energies of ions of different sizes and compare the values obtained in experiments. We first present the theory of solute-solvent couplings in ϕ-FHD equations and then the simulation details and results. For notational simplicity, the formulae are presented for monatomic solutes. Nevertheless, it is straightforward to generalize the simulation framework to flexible polyatomic solutes.

1. Solute-solvent couplings in ϕ-FHD

The interactions between particulate degrees of freedom and field variables are composed of two parts for describing the solvation phenomena. The first part accounts for the volume exclusion between particles and solvent fields through the free energy functionals reported in Ref. 32. Briefly, the non-electrostatic free energy density of the hybrid system is modeled as a functional of the fluid mass density that depends on the overlapped space between each particle and the surrounding grid cells,

$$F[\rho(\mathbf{x})] = \int \left\{ \frac{C}{2}(\rho(\mathbf{x}) - \rho_0)^2 \rho(\mathbf{x})^2 + \frac{m}{2}(\nabla\rho(\mathbf{x}))^2 + \sum_i \frac{k(R_i)}{2} H(R_i - |\mathbf{x} - \mathbf{r}_i|)^2 \rho(\mathbf{x})^2 \right\} d^3\mathbf{x}. \quad (18)$$

The first term in the integral is the two-phase equation of state of a homogeneous fluid and C parameterizes the barrier height between the vapor and the liquid states. The second term represents the surface tension contribution to free energy of an inhomogeneous fluid and m is the proportional constant of the square gradient term. H in the third term is the Heaviside step function representing the volume occupied by the ith particle around its center $\mathbf{r}_i$. R_i is the radius of the particle and $k(R_i)$ denotes the strength of free-energy cost for particles of the size to overlap with the solvent. When discretized, H turns into the fractional extent to which the grid cell at $\mathbf{x}$ is occupied by the sphere of radius R_i centered on the $\mathbf{r}_i$. The values of $C = 900$ amu^{-3} ps^{-2} Å^8, $m = 1100$ amu^{-1} Å^4, and the $k(R_i)$ profile (Table I) parametrized by reproducing the solvation free energies of neutral hard spheres that represent hydrophobic solutes[32] are employed in this work.

TABLE I. Values $k(R)$ in units of amu^{-1} ps^{-2} Å^2 employed in this work.[32]

R/Å	$k(R)$
1.25	1023.75
1.50	1012.50
1.75	1001.25
2.00	990.00
2.25	879.55

The second part of solute-solvent coupling is electrostatic interactions. We introduce the solute charge density, formulated for the charges $\{z_i\}$ and the corresponding positions $\{\mathbf{r}_i\}$ of the ionic species indexed by i as

$$\widetilde{n}_\pm(\mathbf{x}) = \sum_i z_i \delta(\mathbf{x} - \mathbf{r}_i). \quad (19)$$

The subscript $\pm$ indicates that $\widetilde{n}_\pm$ comes from ionic species in contrast to the solvent polarization charge density of Eq. (6). The contribution of ionic particles to the total electric potential is then obtained by solving

$$\nabla^2\phi_\pm = -\frac{\widetilde{n}_\pm}{\varepsilon_0}. \quad (20)$$

With these additions, the divergence of the solvent reversible stress tensor of Eq. (3) is modified to become

$$\nabla\cdot\mathbf{R} = c^2\nabla\rho + \widetilde{n}(\nabla\phi + \nabla\phi_\pm) + \rho\nabla\left(\frac{\delta F}{\delta\rho}\right), \quad (21)$$

where $\delta/\delta\rho$ indicates a functional derivative with respect to ρ.

2. Hydration free energies of ions

To illustrate the unique feature of ϕ-FHD equations in integrating electrostatics with other relevant physical forces in a coarse grained, hybrid particle-field simulation, we consider the hydration of an ion in the ϕ-FHD water model with the polarizability value of $\alpha = 1.325 \times 10^{-3}$ amu^{-1} e^2 ps^2 reported in Sec. III A based on the experimental data of the water dielectric function. An ion i of charge z_i and radius R_i is placed in a box of this water of $61.5 \times 61.5 \times 61.5$ Å^3 in size with the grid spacing of $d_c = 5.125$ Å. We start by considering the solvation of a point particle that only interacts with the polarizable solvent electrostatically. For particles with a finite size, the effects described by the terms in Eq. (18) of the solvent will then be coupled with electrical polarizability in determining the behaviors of solvation. The thermodynamic condition is 300 K and 1 atm in all of the calculations reported here.

The free energy of hydration as a function of (z_i, k_i) is calculated through the perturbation formula,[55]

$$\Delta A_i(z_i, k_i) = -kT \ln\langle e^{-\Delta^{0,0}_{z_i,k_i} U/kT}\rangle_1. \quad (22)$$

Here, $\langle . \rangle_1$ denotes an average in the reference ensemble of the solvated ion and $\Delta^{0,0}_{z_i,k_i} U$ is the energy cost of decoupling the ion from interacting with the solvent,

$$\Delta^{0,0}_{z_i,k_i} U = -\int\left(\frac{V_c k_i}{2} H(R_i - |\mathbf{x} - \mathbf{r}_i|)^2 \rho(\mathbf{x})^2 + z_i \phi(\mathbf{x}) \delta(\mathbf{x} - \mathbf{r}_i)\right) \mathrm{d}^3\mathbf{x}, \quad k_i \equiv k(R_i). \quad (23)$$

In other words, the *Gedanken* process of letting z_i and k_i going to zero is employed for calculating the solvation free energy. This process was subdivided into 10 separate steps, and averaged for a 2 ns trajectory at each step. Further refinement of step number does not alter the resulting values of the free energy. In all calculations, the ion was kept fixed.

In the ϕ-FHD model, the solvent and solute charge densities are resolved on grid cells and the Poisson equation is solved on the discrete points to obtain the electrical potential. Therefore, to properly interpret the contributions from the electrostatic interactions to the free energy of hydration, comparison of the value of the numerical solution with an analytical theory is beneficial. With a zero radius, a monovalent ion is found to have a free energy of hydration of $(159.4 \pm 0.5)k_B T$ at $T = 300$ K. This value corresponds to the solvation free energy of an ion of 1.8 Å Born radius according to the Born solvation model.[56] Even though the ion is treated as a point particle, the finite resolution of discretization imposes an effective size. This size is expected to be smaller than the grid size, since the polarization density in the grid cell with the staggered discretization shown in Figure 1 will respond to the charge of the particle. The empirical value of 1.8 Å Born radius with the point-particle ion is thus consistent with the numerical scheme we devised for solving the ϕ-FHD equations.

Since ions have finite sizes, excluded volume and interfacial effects also contribute to the solvation free energy and these essential forces can be included in ϕ-FHD equations as in the functional of Eq. (18) to couple with the electrical forces due to charges and dipole moments. Combining these universal physical interactions not only makes the origin of peculiar behaviors transparent; it also provides a solid foundation for transferability of model parametrization across different cases. In the following, we illustrate that the solvent polarizability obtained in Sec. III A based on the experimental dielectric function of water and the non-electrostatic parameters obtained from capturing the solvation free energies of neutral solutes via Eq. (18)[32] can be put together to describe ion hydration free energies without adding new terms to the free energy functional.

After specifying the radius of an ion, the free-energy functional of solute-solvent interactions in Eq. (18) can be combined with the electrical part to compute the hydration free energy via Eqs. (22) and (23). Figure 4 plots the resulting value as a function of the ion radius used in solving the ϕ-FHD equations. In this figure, the loci of the experimental

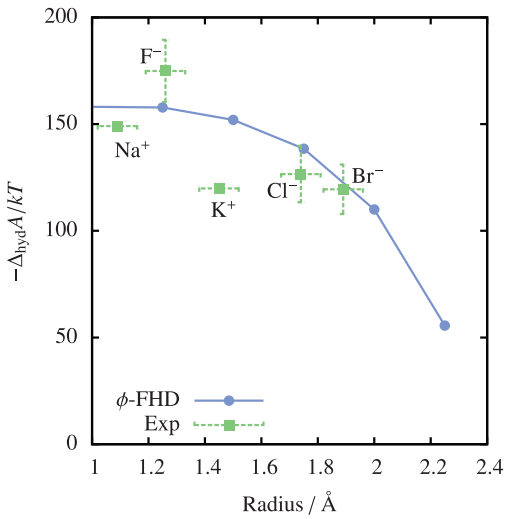

FIG. 4. Plot of the free energy of hydration of a select number of monovalent ions as a function of their radius for the ϕ-FHD simulations and experimental results using crystallographic radii.[57–60] The uncertainty in the crystallographic radii stems from the choice of radius for the O^{2-} ion by which the data is normalized. The uncertainty for the free energies of hydration is the standard deviation of three independent measurements. Following earlier authors,[57,61] all of these measurements have been adjusted to the scale where the hydrogen ion has a free energy of hydration of 1050 kJ/mol, to be internally consistent.

values of the hydration free energies of common ions are also labeled at the crystallographic radii reported by Shannon[60] to represent a reference distribution of hydration free energy versus ion size that purely based on experiments without referring to a theory. It can be seen in Figure 4 that the ϕ-FHD profile agrees well with experimental values. Therefore, without fine-tuning, the balance of electrostatic and non-electrostatic interactions in the ϕ-FHD equations can capture the behavior of ion hydration semi-quantitatively.

To account for the incomplete ability of resolving the molecular details of liquid structures in this CG scale and make the results in quantitative agreement to the targeted values, additional forms of solvent-solute interactions may be included in the ϕ-FHD framework. Another approach is using parameters in the current free-energy functional to effectively incorporate the effects of molecularly specific interactions. For example, the size of ions used in the hybrid simulation can be determined by the corresponding values of experimental hydration free energy to set the ϕ-FHD radii of ions. Comparing the values with other commonly used definitions of atomic radius, such as the crystallographic and effective radii of Shannon[60] and the van der Waal radii of molecular mechanical force field, Table II indicates that the so-calculated ϕ-FHD radii are in a similar range. Therefore, the strategy of ϕ-FHD in integrating essential forces in the mesoscopic scale simulation gives rise to physically reasonable parameters of ionic species.

For a small ion such as fluoride, though, the electrostatic coupling with the solvent is very strong and the solvation free energy is under-predicted by the ϕ-FHD equations since the grid cell size of 5 Å used for resolving the charge distribution is relatively coarse. As pointed out earlier, the finite-size discretization in ϕ-FHD equations introduces an effective

TABLE II. Effective ionic radii in units of Å.

	Shannon[a]		ϕ-FHD	
	"Crystal"	"Effective"	($d_c = 5.125$ Å)	Beglov and Roux[b]
F^-	1.19	1.33	...	...
Cl^-	1.67	1.81	1.89	2.27
Br^-	1.82	1.96	1.94	...
Na^-	1.16	1.02	1.57	1.36
K^+	1.52	1.38	1.94	1.76

[a]"Crystal" and "effective" ionic radii from Ref. 60.
[b]CHARMM27 Lennard-Jones radii fitted to solvation free energies.[62]

radius of 1.8 Å even for a point-particle ion. Furthermore, the details of molecular structures are not explicitly represented. In this case, the relatively moderate discrepancy to the experimental observable can be overcome by increasing the apparent charge of very small ions if necessary or incorporating an additional term representing the effect of molecularly specific solute-solvent interactions and liquid structures.

3. Radial dependence of ion hydration free energy in a nano droplet

With the flexibility of particle-field coupling and versatility of incorporating different interaction forces, the ϕ-FHD equations can be readily applied to go beyond bulk simulations. As an illustration, we consider the hydration free energy of an ion as a function of its radial distance to the center of a spherical water droplet of 25 Å. Since droplets of around this size only exist transiently before merging into an extended liquid region, it is difficult to study their properties such as solvation that play important roles in determining the structures and dynamics observed at a larger and longer scale. In ϕ-FHD, a droplet of this size can be formed with the following free-energy functional.

$$F_{\text{drop}}[\rho(\mathbf{x})] = \int \left\{ \frac{C}{2}(\rho(\mathbf{x}) - \rho_0)^2 \rho(\mathbf{x})^2 + \frac{m}{2}(\nabla\rho(\mathbf{x}))^2 + \frac{\kappa}{2} f(\mathbf{x})^2 \rho(\mathbf{x})^2 \right\} d^3\mathbf{x}. \quad (24)$$

This equation is analogous to Eq. (18) with the only difference in the third term that forms the cavity of the excluded volume of a particle in Eq. (18). In Eq. (24), $f(\mathbf{x})$ takes the following form to keep the droplet around the origin of the simulation cell with the size of 107.625^3 Å^3.

$$f(\mathbf{x}) = \begin{cases} 0 & \text{if } |\mathbf{x}| < 25 \\ 1 - e^{-0.04(|\mathbf{x}|-25)^2} & \text{otherwise} \end{cases}. \quad (25)$$

Here, the values of C, m, κ in Eq. (24) are taken as the same as those in Eq. (18) that were parametrized to reproduce the solvation free energies of neutral hydrophobic particles.[32] This approach sets $\kappa = 216$ amu^{-1} ps^{-2} Å^2. The dynamics of the polarization density in grid cells of 5 Å and their electrostatic effects are propagated by the ϕ-FHD equations along with the dynamics of other fields in the droplet system at 300 K. A plot of the averaged density profile is shown in Figure 5 that illustrates the phase boundary of the droplet from which the Gibbs dividing surface is determined to locate at $r = 24.6$ Å from the droplet center. The hydration free energy of an ion is computed at different positions in the droplet via the protocol described in Sec. III B 2.

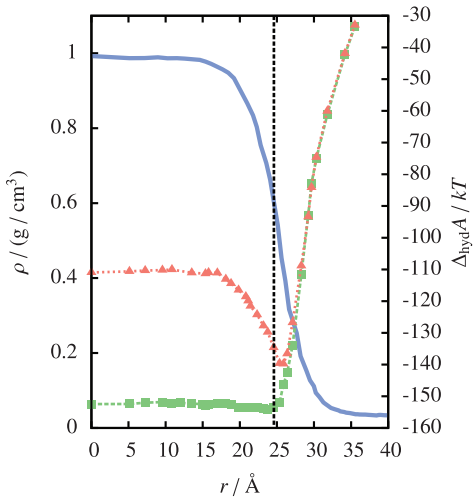

FIG. 5. Density profile of the water droplet and its saturated vapor (solid blue line, left ordinate axis) and free energy profile of a monovalent ion of radius 1.5 Å (green squares, dashed connector, right ordinate axis), and 2.0 Å (red triangles, dotted connector, right ordinate axis), all as a function of the distance, r, from the droplet center at $T = 300$ K. The Gibbs dividing surface is indicated by the dashed vertical black line.

With dielectric responses mediated through the polarization density of the solvent, electrostatic interactions will impose favorable hydration free energy of the particle. On the other hand, the free energy cost of cavity formation and surface tension for the solvent to surround the ion disfavors solvation. Therefore, the free energy of hydration of the ion will be a strong function of its radial distance from the droplet center, r, especially when the ion is near the vapor-liquid interface of the droplet. This dependence of hydration free energy on r is also expected to be sensitive to the size of the particle that influences both the electrostatic and non-electrostatic energies. For the droplet of 25 Å we found that for an ion with the radius less than 1.5 Å, it prefers to stay inside of the droplet as shown in Figure 5. For an ion with a larger radius of 2.0 Å Figure 5 illustrates that the free energy of hydration can indeed be lower at the droplet interface. Therefore, we conclude from ϕ-FHD simulation that ions of a sufficient size can serve to stabilize the surface energy of a nano droplet. Experimental observation of ion enrichment at a water-vapor interface systems has also been reported.[63] It is also recognized that ϕ-FHD equations can be applied to inhomogeneous systems at the nanoscale to capture various specific behaviors by putting together the relevant forms of physical forces.

C. Coarse graining an all-atom simulation into the ϕ-FHD model

In previous examples, we show that experimental information like solvent dielectric function and hydration free energies of ions can be employed to determine the model

parameters of ϕ-FHD equations. Such fundamental properties may also be calculated from detailed molecular simulations. The solvation free energies of neutral particles[64] for setting the parameters of the non-electrostatic free energy functional of Eq. (18)[32] is another clear example. Although in these cases the properties averaged over the entire length-scale of the system can be combined in the ϕ-FHD framework to model the behaviors of more complex systems, it is highly desirable if the mesoscopic model could also be interfaced at the fundamental length-scale of grid cells. In analogous to the parametrization of all-atom molecular mechanical forces fields for which quantum mechanical calculations play a pivotal role in imposing the accuracy and predicability in the coarser representation of molecular mechanics, it is important to establish whether the mesoscopic ϕ-FHD equations could be bridged to simulation models with full atomistic details. This capability can help to develop and parametrize the ϕ-FHD model at the finest possible scale by taking information from a finer-grained model that resolves molecular details. With respect to all-atom molecular dynamics simulation, the trans-scale connection can also serve as an analysis tool for capturing the emergent properties at the mesoscopic scale based on the ϕ-FHD equations.

In this section, we consider coarse graining an all-atom MD simulation into the representation of ϕ-FHD equations. For FHD equations without the electrical forces due to dipole moments and charges, we have shown that the position and velocity vectors of atoms in a molecular system can be mapped to field variables in grid cells for direct comparison with the results of a FHD simulation. The statistics of the field variables computed from the all-atom MD simulation can then be employed to determine the parameters of thermodynamics and transport phenomena. When the two simulation models at different resolutions use with the same parameters of thermodynamics and dynamics and their resulting fluctuations and relaxation of the corresponding field variables agree with each other, it is established that all-atom MD and FHD is compatible.

We found that the compatibility of FHD with all-atom MD can be achieved with grid cells as small as 5 Å if the finite sizes of molecules are accounted for when mapping their positions onto Eulerian grid cells. Each molecule such as a water is assumed to have an effective volume in which the mass density is uniformly distributed. Given the grid cells that have an overlapped volume with the molecule, the field variable due to its existence such as density, kinetic energy, and velocity, etc. can be assigned to those grid cells according to the fractional volumes of the particle that they contain. If the grid cell size is sufficiently large with respect to the molecular size (beyond 10–15 Å for water), this scheme of continuous particle-to-field mapping does not affect the result and the particle can be treated as a point and assigned to whichever cell it is within. When the size of grid cells becomes small and approaches to a molecular resolution, the statistics of field fluctuations mapped from all-atom MD become sensitive to the effective size of the particle. The particle size can thus be used as an adjustable parameter to reach the aforementioned compatibility between all-atom MD and FHD. For example, using the effective volume of a water molecule as a cubic of 2.4 Å in each side to compute density fields from atomic positions and masses can reach agreement in the density fluctuations with FHD simulation at the grid cell size of 5 Å under the same isothermal compressibility at 300 K and 1 atm. It was also found for the statistics of various types of field variables to reach compatibility, the optimal sizes of particle-to-filed mapping are distinct in different cases.

For the ϕ-FHD equations that include electrical forces due to solvent polarizability, we aim to utilize the statics of dipole moment fluctuations calculated from the trajectory of an all-atom MD simulation to analyze the effects of coarse graining away molecular details. The core objective is to characterize how the *Ansatz* of Eq. (10) and the electrical free energy functional of Eq. (7) capture the local dipole moment fluctuations in a molecular fluid. Equation (7) involves a term representing the energetic response of the dipole moment density in a grid cell to the local electrical field. Therefore, unlike the other field variables in ϕ-FHD that the equation of state or constitutive relationships are directly input to the dynamics equation, Eq. (7) and the concomitant dynamics of Eq. (10) are coupled with the Poisson equation of Eq. (9) in determining the electrical forces. The connection between the constitutive parameters such as polarizability α and the statistics of local dipole moment fluctuations is thus indirect and nonlinear in the ϕ-FHD equations. This unique feature of electrical responses represents a key challenge in computing the model parameters of ϕ-FHD from all-atom MD trajectories.

Another term in Eq. (7) is the electrical energy due to the dipole moment vector in a grid cell assuming a non-zero value that gives rises to the constitutive equation of the dielectric response at equilibrium in Eq. (8). Therefore, the correlation between dipole moments of different grid cells in ϕ-FHD comes solely from electrostatic coupling, although it is expected that molecular structures and interactions will also contribute to couple local dipole moments. This issue will be analyzed quantitatively based on the trajectory of an all-atom simulation for which the details are presented first in the following.

1. The details of all-atom MD for generating the reference trajectory

We consider 7773 `TIP3P`[65] water molecules in a cubic box of 61.5 Å in length corresponding to the density of liquid water at ambient conditions. The NVT simulation of this system with periodic boundary conditions was performed using the `GROMACS 4.6.3` software.[66] The leap-frog integrator with a 2 fs time step was employed and the bond lengths and angle of each water molecule were constrained at the parameter values using the LINCS algorithm.[67] Lennard-Jones interactions were truncated and shifted with a cutoff of 10 Å and a fourth-order particle mesh Ewald summation with a 1.0 Å grid spacing was used to calculate electrostatic interactions. After equilibration, a trajectory of 120 ns was generated at 300 K using the Nosé-Hoover thermostat. The center-of-mass velocity was reset to zero at intervals of 200 fs.

2. Local dipole moment fluctuations in all-atom MD and ϕ-FHD

By discretizing the simulation box of all-atom MD with 12^3 cubic grid cells of 5.125 Å, the density, velocity, and polarization density on these Eulerian grid cells can be calculated from the positions and velocities of atoms in the MD trajectory. The dipole moment vector of each water molecule is calculated from the atomic partial charges in the molecular mechanical force field and the configuration of each snapshot and is placed at the water center of mass. For electrostatics, if each water molecule is coarse grained into a cubic box centered at the center of mass with the length d_{mol}, the dipole moment density of each water molecule is calculated as the dipole moment vector divided by d_{mol}^3. That is, the water dipole moment is assumed to uniformly distribute within the molecule volume specified by d_{mol}. In the case of $d_{\text{mol}} = 0$, water molecules are coarse grained into point particles and the dipole moment vector calculated from molecular structures and partial charges is a point dipole at the center of mass. The dipole moment of each water molecule is then assigned to the overlapping grid cells fixed in space in proportional to the volume fractions of the d_{mol}^3 cubic of each water in different grid cells. For $d_{\text{mol}} = 0$, the point dipole of a water molecule is assigned to the grid cell that contains its center of mass. Therefore, after specifying d_{mol}, the all-atom MD trajectory is converted into a series of configurations for the polarization density in Eulerian grid cells.

With the movements of atoms, the corresponding fluctuations of the coarse-grained polarization density distributed in Eulerian grid cells are calculated from the all-atom MD trajectory according to the procedure described above. Given a set of parameters in the ϕ-FHD equations with identical sizes of the simulation system and grid cells as well as the same the thermodynamic conditions, the fluctuations of dipole moment density on grid cells can be calculated for the two models to be compared and matched.

First, we consider the total polarization density of the entire simulation box, $\mathbf{p}_{\text{tot}}$, which is the sum of all dipole moment densities in grid cells. The second moment of the fluctuations of $\mathbf{p}_{\text{tot}}$, $\langle \mathbf{p}_{\text{tot}}^2 \rangle$, is approximately related to the static dielectric constant of the system[68] as

$$\widehat{\varepsilon}(0) - 1 = \frac{\widehat{\varepsilon}(0)}{2\widehat{\varepsilon}(0) + 1} \frac{V \langle \mathbf{p}_{\text{tot}}^2 \rangle}{\varepsilon_0 k_{\text{B}} T}. \tag{26}$$

Therefore, by adjusting α, we can match the value of $\langle \mathbf{p}_{\text{tot}}^2 \rangle$ observed in ϕ-FHD to that calculated from the all-atom MD trajectory. Since the value of $\langle \mathbf{p}_{\text{tot}}^2 \rangle$ is independent of d_{mol} as the mapping procedure preserves the total dipole moment in the simulation box, the value of α is unambiguously determined in this approach. The resulting value of α is 1.71×10^{-3} amu^{-1} e^2 ps^2, larger than the value of fitting experimental dielectric function in Sec. III A due to the 25% overestimation of the static dielectric constant of TIP3P water.[69] Next, we compare the value of the variance of local polarization density averaged over grid cells, $\langle \mathbf{p}^2 \rangle$, of ϕ-FHD and all-atom MD under the same α and hence the matched value of $\langle \mathbf{p}_{\text{tot}}^2 \rangle$.

The agreement in total dipole moment fluctuations equates the α values of all-atom MD and ϕ-FHD. The comparison of $\langle \mathbf{p}^2 \rangle$ at the length-scale of grid cells will thus inform the effects of the molecular details missed by Eq. (7). This equation is formulated by letting the dielectric constitutive equation of Eq. (8) emerge without considering the potential effects of molecular details on local dipole moment fluctuations. The value of $\langle \mathbf{p}^2 \rangle$ calculated from all-atom MD depends on the d_{mol} value used in the atom-to-field mapping discussed earlier and the corresponding $\langle \mathbf{p}^2 \rangle = 9.21 \times 10^{-5}$ e^2/Å^4 at $d_{\text{mol}} = 0$ is the upper bound of local fluctuations of dipole moment densities estimated in all-atom MD. The resulting value of $\langle \mathbf{p}^2 \rangle$ in ϕ-FHD simulation at the same α value, though, is significantly higher at 2.12×10^{-4} e^2/Å^4. This difference cannot be remedied by adjusting d_{mol} as a nonzero value of which will only lower $\langle \mathbf{p}^2 \rangle$ in the calculation from all-atom MD and move it further away from the ϕ-FHD value.

This result indicates that under the same values of $\langle \mathbf{p}_{\text{tot}}^2 \rangle$ and solvent polarizability, the regularization of local dipole moment fluctuations by the molecular details encoded in the all-atom MD is higher than that described by Eq. (7). This equation of local electrical energy density considers the static dielectric response via α and can capture the solvent dielectric function with the transport coefficient η in the equation of motion of Eq. (10) as discussed in Sec. III A. However, the static correlations between dipole moment densities in different cells are not explicitly accounted for. Coupling terms between dipole moment densities thus need to be added to Eq. (7). The parameters of this correlational energy $U_{\text{cor}}[\mathbf{p}]$ will be determined by matching with the values of local fluctuations observed in all-atom MD. The values of η and α will remain unchanged to retain the frequency-dependent as well as static dielectric responses of the solvent. For the range of values of coupling parameters that we have investigated here, simulation results indicate that the dielectric function of the solvent is not affected by adding $U_{\text{cor}}[\mathbf{p}]$ to Eq. (7) as expected from the equation of motion of Eq. (10).

For a grid cell i, its neighbors are categorized into three groups. Since the simulation system and the grid cells are cubic, the discretization forms a cubic lattice. For grid cell i, NN(i) is the set of nearest neighbors (von Neumann neighborhood) that the cell shares a common surface with; NNN(i) is the set of the second-nearest neighbors that the cell shares a common line with; and the set NNNN(i) constitutes the third-nearest neighbors (which in union with the previous sets makes up the Moore neighborhood) that the cell shares a common corner point with. The results of analysis shown in the following indicate that involving the second shell correlations of grid cells in generalizing the polarization free energy functional is not necessary.

Table III lists the averaged values of $\langle \mathbf{p}^2 \rangle$ and $\langle (\mathbf{p}_i - \mathbf{p}_j)^2 \rangle$ calculated in all-atom MD and ϕ-FHD simulations. It can be seen clearly that the local dipole moment fluctuations and correlations are overestimated by the ϕ-FHD equations with Eq. (7) that is denoted as ϕ-FHD(s) in Table III. Since there is no additional parameter in the equation to modulate the values of local dipole moment fluctuations, Eq. (7) needs to be augmented to capture the phenomena in all-atom MD.

TABLE III. Values of characteristic equilibrium functions of the polarization density as given by AA-MD and ϕ-FHD simulations, both simple and extended. Variances are given in units of $e^2/\text{Å}^4$. The grid cell spacing is $d_c = 5.125$ Å.

	AA-MD	ϕ-FHD(s)	ϕ-FHD(e)
Var($\mathbf{p}$)	9.21×10^{-5}	2.12×10^{-4}	9.14×10^{-5}
Var($\mathbf{p}_i - \mathbf{p}_j$)...			
$i \in$ NN(j)	1.62×10^{-4}	4.24×10^{-4}	1.62×10^{-4}
$i \in$ NNN(j)	1.78×10^{-4}	4.24×10^{-4}	1.78×10^{-4}
$i \in$ NNNN(j)	1.82×10^{-4}	4.24×10^{-4}	1.82×10^{-4}

Therefore, the correlational energy $U_{\text{cor}}[\mathbf{p}]$ is added to Eq. (7) and the total free energy functional of the dipole moment fields $U[\mathbf{p}]$ becomes

$$U[\mathbf{p}] = \int u\big(\mathbf{p}(\mathbf{x})\big) d^3\mathbf{x} + U_{\text{cor}}[\mathbf{p}]. \tag{27}$$

In principle, the local dipole-dipole correlations can be recaptured if the model is extended with the proper energy function.

Since the local fluctuations of electric fields are more restricted and dipole couplings between neighboring cells are stronger in all-atom MD, the $U_{\text{cor}}[\mathbf{p}]$ term ought to impose restraints in the deviation of dipole moment density fields between neighboring grid cells. Therefore, to capture such phenomena, we impose the simple form of harmonic coupling between polarization densities as the starting point:

$$U_{\text{cor.}}[\mathbf{p}] = \sum_{i=1}^{N_c} \left\{ \frac{k_1}{2} \sum_{j \in \text{NN}(i)} (\mathbf{p}_i - \mathbf{p}_j)^2 + \frac{k_2}{2} \sum_{j \in \text{NNN}(i)} (\mathbf{p}_i - \mathbf{p}_j)^2 + \dots \right\}. \tag{28}$$

With $U_{\text{cor.}}$ added to Eq. (7), the dynamics of the dipole moment densities of Eq. (10) or Eq. (12) now experience the additional forces of

$$-\frac{\delta U_{\text{cor}}}{\delta \mathbf{p}_i} = -k_1 \sum_{j \in \text{NN}(i)} (\mathbf{p}_i - \mathbf{p}_j) - k_2 \sum_{j \in \text{NNN}(i)} (\mathbf{p}_i - \mathbf{p}_j) - \dots \tag{29}$$

in the discretized analogs of Eqs. (10) and (12). Here i is the index of an arbitrary grid cell and corresponds to $\mathbf{x}$ in the continuum description in which those equations are presented. Therefore, only the constitutive equation of dipole moment densities is changed and the rest of ϕ-FHD equations remain unchanged. An essential test of this approach of modelling the free energy functional of dipole moment densities is whether adjusting the values of k_1 to k_3 can reproduce the values of $\langle(\mathbf{p}_i - \mathbf{p}_j)^2\rangle$ observed in all-atom MD and see if the value of $\langle \mathbf{p}^2 \rangle$ can also be captured while keeping $\langle \mathbf{p}_{\text{tot}}^2 \rangle$ unchanged. Through a least-square minimization of the differences in $\langle(\mathbf{p}_i - \mathbf{p}_j)^2\rangle$ between the first, second, and third nearest neighbors of grid cells, the optimal values of k_1, k_2 and k_3 are listed in Table IV in which the results of the extended ϕ-FHD equations with Eq. (28) is denoted as ϕ-FHD(e).

Table III indicates that the values of $\langle(\mathbf{p}_i - \mathbf{p}_j)^2\rangle$ calculated from all-atom MD can be matched by the ϕ-FHD equations with the functional of dipole moment density extended to incorporate local couplings. At the grid cell size of 5.125 Å for water, only the couplings to the first nearest neighbors of grid cells assume a significant value and the force constants of the second and third nearest neighbors are much smaller as Table IV shows. Although the force constant values calculated by matching local correlations of dipole moments will depend on the level of coarse graining dictated in this case by the grid cell size, the ϕ-FHD framework allows the values to be determined from the statics calculated from the all-atom MD trajectory. Furthermore, we note that $\langle \mathbf{p}_{\text{tot}}^2 \rangle$ remains invariant with respect to the matching of the local dipole moment fluctuations. Therefore, the ϕ-FHD equations developed in this work can describe the macroscopic property of dielectric response as well as the molecularly specific behaviors of local fluctuations and correlations of dipole moments in the solvent.

TABLE IV. Specification of the parameterization of the extended ϕ-FHD model for TIP3P water. In both cases $\alpha = 1.71 \times 10^{-3}$ amu^{-1} e^2 ps^2.

$k_1\alpha/\text{Å}^6$	13.68
$k_2\alpha/\text{Å}^6$	0.5228
$k_3\alpha/\text{Å}^6$	− 0.6609

IV. CONCLUSION

In developing a theoretical framework for mesoscopic scale simulation, we show for the first time that the electrical forces due to interactions between charged and dipolar species can be incorporated into the equations of fluctuating hydrodynamics. For the electrostatic potential ϕ due to fluctuations of dipole moments in the solvent, an *Ansatz* of dynamics of dipole moment densities was devised in Eq. (10) based on the constitutive equation of dielectric response of Eq. (8) and the phenomenological principle of fluctuation-dissipation balance. For the resulting ϕ-FHD equations, the scaling of computation time is $\mathcal{O}(N \log N)$ with the system size by using a fast Fourier transform to solve the Poisson equation of ϕ. Therefore, the ϕ-FHD framework can serve as a platform to integrate the essential forces, including hydrodynamics and hydrophobicity in addition to electrostatics, that govern the emergent behaviors of molecular systems at the nanoscale. This unique capability is illustrated by showing that the dielectric function of water and hydration free energies of ions in homogeneous and heterogeneous environments can be calculated via mesoscopic simulation. We also establish that the ϕ-FHD representation can be coarse grained from all-atom MD simulation by generalizing the electrical free energy functional as in Eq. (27) and Eq. (28) to capture the specific behaviors due to the molecular details not explicitly considered. The field variables in ϕ-FHD equations can thus be mapped from a finer-grained simulation for model development and parametrization. Therefore, the ϕ-FHD method presented in this work has promising potential as a useful tool at an intermediate scale for the multiscale modeling and simulation of complex molecular systems such as protein machines and nanofluidic phenomena.

ACKNOWLEDGMENTS

This work was supported by the National Chiao Tung University, Taiwan. The funding from the Ministry of Science and Technology of Taiwan, Taiwan via Grant Nos. 102-281-B-009-005-, 102-2113-M-009-022-MY2, and 103-2628-M-009-003-MY3 is acknowledged.

APPENDIX: ELECTROSTATIC CONTRIBUTION TO THE DIVERGENCE OF THE REVERSIBLE STRESS TENSOR IN THE ϕ-FHD EQUATIONS

For a free energy density functional $f[\theta_1, \theta_2, \ldots] = \partial F[\theta_1, \theta_2, \ldots]/\partial V$, depending on the densities $\{\theta_i\}$ of different components, the divergence of the reversible stress tensor is defined as[30]

$$\nabla \cdot \mathbf{R} = -\sum_i \theta_i \nabla \left(\frac{\delta f[\theta_1, \theta_2, \ldots]}{\delta \theta_i} \right). \tag{A1}$$

Here, we focus on the electrostatic contributions (neglecting magnetic effects), and F is thus written as

$$F[\rho, \widetilde{n}] = F_\rho[\rho] + F_C[\widetilde{n}]. \tag{A2}$$

In this form, we assume that the electrostatic component to the free energy is separable from the other forces. We assume that the non-electrostatic part of the divergence of the reversible stress tensor is adequately given by some known expression, for instance, from an equation of state or derived from a free-energy density functional. The Coulombic part is

$$F_C[\widetilde{n}] = \frac{1}{2} \int\int \frac{\widetilde{n}(\mathbf{x})\widetilde{n}(\mathbf{x}')}{4\pi\varepsilon|\mathbf{x}-\mathbf{x}'|} d^3\mathbf{x} d^3\mathbf{x}', \tag{A3}$$

and the corresponding free energy density at $\mathbf{x}$ is then

$$f_C[\widetilde{n}(\mathbf{x})] = \frac{1}{2} \int \frac{\widetilde{n}(\mathbf{x})\widetilde{n}(\mathbf{x}')}{4\pi\varepsilon|\mathbf{x}-\mathbf{x}'|} d^3\mathbf{x}'. \tag{A4}$$

Taking the functional derivative with respect to the charge density, we have

$$\frac{\delta f_C}{\delta \widetilde{n}} = \int \frac{\widetilde{n}(\mathbf{x}')}{4\pi\varepsilon|\mathbf{x}-\mathbf{x}'|} d^3\mathbf{x}' \tag{A5}$$

and then taking the gradient with respect to $\mathbf{x}$ yields

$$\nabla \left(\frac{\delta f_C}{\delta \widetilde{n}} \right) = -\int \frac{\widetilde{n}(\mathbf{x}')}{4\pi\varepsilon|\mathbf{x}-\mathbf{x}'|^3} (\mathbf{x}-\mathbf{x}') d^3\mathbf{x}'. \tag{A6}$$

Clearly, this equation is the definition of the electrostatic field, so that when inserted into Eq. (A1), the electrostatic contribution to the divergence of the reversible stress tensor is obtained as the second term in Eq. (3).

[1] R. J. White and A. D. Sharrocks, Trends Genet. **26**, 214 (2010).
[2] S. Klinge, F. Voigts-Hoffmann, M. Leibundgut, S. Arpagaus, and N. Ban, Science **18**, 941 (2011).
[3] J. Bauer, K. Chen, A. Hiltbunner, E. Wehrli, M. Eugster, D. Schnell, and F. Kessler, Nature **403**, 203–207 (2000).
[4] C. Somerville, Annu. Rev. Cell Dev. Biol. **22**, 53 (2006).
[5] J. P. Changeux, Science **308**, 1424 (2005).
[6] M. Muthukumar, Annu. Rev. Biophys. Biomol. Struct. **36**, 435 (2007).
[7] R. D. Groot, Langmuir **16**, 7493–7502 (2000).
[8] S. R. Euston, Curr. Opin. Colloid Interface Sci. **9**, 321–327 (2004).
[9] I. Pagonabarraga, B. Rotenberg, and D. Frenkel, Phys. Chem. Chem. Phys. **12**, 9566 (2010).
[10] W. G. Noid, J.-W. Chu, G. S. Ayton, V. Krishna, S. Izvekov, G. A. Voth, A. Das, and H. C. Andersen, J. Chem. Phys. **128**, 244114 (2008).
[11] H. M. Cho and J.-W. Chu, J. Chem. Phys. **131**, 134107 (2009).
[12] J. S. Rowlinson, and B. Widom, in *Molecular Theory of Capillarity* (Dover Publications, New York, 2002).
[13] M. Kardar, *Statistical Mechanics of Fields* (Cambridge University Press, 2007).
[14] L. Landau and E. Lifshitz, *Fluid Mechanics* (Pergamon, 1959).
[15] J. M. O. Zárate and J. V. Sengers, *Hydrodynamic Fluctuations in Fluids and Fluid Mixtures* (Elsevier, New York, 2006).
[16] P. Español and M. Revenga, Phys. Rev. E **67**, 026705 (2003).
[17] D. Moroni, B. Rotenberg, J.-P. Hansen, S. Succi, and S. Melchionna, Phys. Rev. E **73**, 066707 (2006).
[18] G.-R. Liu and M. Liu, *Smoothed Particle Hydrodynamics: A Meshfree Particle Method* (World Scientific, 2003).
[19] J. J. Monaghan, Rep. Prog. Phys. **68**, 1703 (2005).
[20] P. Hoogerbrugge and J. Koelman, EPL (Europhys. Lett.) **19**, 155 (1992).
[21] J. Koelman and P. Hoogerbrugge, EPL (Europhys. Lett.) **21**, 363 (1993).
[22] P. Espanol and P. Warren, EPL (Europhys. Lett.) **30**, 191 (1995).
[23] B. Dünweg, U. D. Schiller, and A. J. C. Ladd, Phys. Rev. E **76**, 036704 (2007).
[24] R. Schmitz and B. Dünweg, J. Phys.: Condens. Matter **24**, 464111 (2012).
[25] F. Balboa, J. B. Bell, R. Delgado-Buscalioni, and A. Donev, Multiscale Model. Simul. **10**, 1369 (2012).
[26] N. K. Voulgarakis and J.-W. Chu, J. Chem. Phys. **130**, 134111 (2009).
[27] N. K. Voulgarakis, S. Satish, and J.-W. Chu, J. Chem. Phys. **131**, 234115 (2009).
[28] J. H. Irving and J. G. Kirkwood, J. Chem. Phys. **18**, 817 (1950).
[29] D. J. Evans and G. P. Morriss, *Statistical Mechanics of Non-Equilibrium Liquids* (Academic, 1990).
[30] B. Z. Shang, N. K. Voulgarakis, and J.-W. Chu, J. Chem. Phys. **137**, 044117 (2012).
[31] B. Z. Shang, N. K. Voulgarakis, and J.-W. Chu, J. Chem. Phys. **135**, 044111 (2011).
[32] N. K. Voulgarakis, B. Z. Shang, and J.-W. Chu, Phys. Rev. E **88**, 023305 (2013).
[33] K. Henjes and M. Liu, Ann. Phys. **223**, 243 (1993).
[34] E. Lee, J.-W. Chu, and J.-P. Hsu, Curr. Opin. Colloid Interface Sci. **205**, 65 (1998).
[35] E. Lee, J.-W. Chu, and J.-P. Hsu, J. Chem. Phys. **110**, 11643 (1999).
[36] J.-W. Chu, W.-H. Lin, E. Lee, and J.-P. Hsu, Langmuir **17**, 6289 (2001).
[37] L. Onsager, J. Am. Chem. Soc. **58**, 1486 (1936).
[38] A. K. Jha and K. F. Freed, J. Chem. Phys. **128**, 034501 (2008).
[39] A. M. Afonso, F. T. Pinho, and M. A. Alves, J. Non-Newtonian Fluid Mech. **179–180**, 55 (2012).
[40] P. Koehl, H. Orland, and M. Delarue, J. Phys. Chem. B **113**, 5694 (2009).
[41] R. de Groot, J. Chem. Phys. **118**, 11265 (2003).
[42] J. Smiatek and F. Schmid, Comput. Phys. Commun. **182**, 1941 (2011).
[43] U. M. B. Marconi and S. Melchionna, J. Chem. Phys. **131**, 014105 (2009).
[44] F. Capuani, I. Pagonabarraga, and D. Frenkel, J. Chem. Phys. **121**, 973 (2004).
[45] I. Pagonabarraga, F. Capuani, and D. Frenkel, Comput. Phys. Commun. **169**, 192 (2005).
[46] F. Capuani, I. Pagonabarraga, and D. Frenkel, J. Chem. Phys. **124**, 124903 (2006).
[47] S. Melchionna, J. Comput. Phys. **230**, 3966 (2011).
[48] U. Marini Bettolo Marconi and S. Melchionna, Langmuir **28**, 13727 (2012).
[49] B. R. Brooks, C. L. Brooks III, A. D. Mackerell, Jr., L. Nilsson, R. J. Petrella, B. Roux, Y. Won, G. Archontis, C. Bartels, S. Boresch, A. Caflisch, L. Caves, Q. Cui, A. R. Dinner, M. Feig, S. Fischer, J. Gao, M. Hodoscek, W. Im, K. Kuczera, T. Lazaridis, J. Ma, V. Ovchinnikov, E. Paci, R. W. Pastor, C. B. Post, J. Z. Pu, M. Schaefer, B. Tidor, R. M. Venable, H. L. Woodcock, X. Wu, W. Yang, D. M. York, and M. Karplus, J. Comput. Chem. **30**, 1545 (2009).
[50] P. H. Hünenberger, Adv. Polymer. Sci. **173**, 105 (2005).
[51] W. M. Deen, *Analysis of Transport Phenomena* (Oxford University Press, New York, 1998).
[52] R. C. Singleton, IEEE Trans. Audio Electroacoust. **17**, 93 (1969).
[53] T. Meissner and F. Wentz, IEEE Trans. Geosci. Electron. **42**, 1836 (2004).
[54] W. B. Floriano and M. A. C. Nascimento, Braz. J. Phys. **34**, 38 (2004).
[55] R. W. Zwanzig, J. Chem. Phys. **22**, 1420 (1954).
[56] M. Born, Z. Phys. **1**, 45 (1920).
[57] Y. Marcus, J. Chem. Soc., Faraday Trans. **87**, 2995 (1991).

[58]H. Friedman, C. Krishnan, and F. Franks, *Water: A Comprehensive Treatise* (Plenum Press, 1973).
[59]B. E. Conway, J. Solution Chem. **7**, 721–770 (1978).
[60]R. Shannon, Acta Crystallogr., Sect. A: Cryst. Phys., Diffr., Theor. Gen. Crystallogr. **32**, 751 (1976).
[61]G. Hummer, L. R. Pratt, and A. E. García, J. Phys. Chem. **100**, 1206 (1996).
[62]D. Beglov and B. Roux, J. Chem. Phys. **100**, 9050 (1994).
[63]D. E. Otten, P. R. Shaffer, P. L. Geissler, and R. J. Saykally, Proc. Natl. Acad. Sci. U. S. A. **109**, 701 (2012).
[64]K. Lum, D. Chandler, and J. D. Weeks, J. Phys. Chem. B **103**, 4570 (1999).
[65]W. L. Jorgensen, J. Chandrasekhar, J. D. Madura, R. W. Impey, and M. L. Klein, J. Chem. Phys. **79**, 926 (1983).
[66]S. Pronk, S. Páll, R. Schulz, P. Larsson, P. Bjelkmar, R. Apostolov, M. R. Shirts, J. C. Smith, P. M. Kasson, D. van der Spoel, B. Hess, and E. Lindahl, Bioinformatics **29**, 845 (2013).
[67]B. Hess, H. Bekker, H. J. C. Berendsen, and J. G. E. M. Fraaije, J. Comput. Chem. **18**, 1463 (1997).
[68]H. Fröhlich, Trans. Faraday Soc. **44**, 238 (1948).
[69]D. van der Spoel, P. J. van Maaren, and H. J. C. Berendsen, J. Chem. Phys. **108**, 10220 (1998).